JACS
JOURNAL OF THE AMERICAN CHEMICAL SOCIETY

Communication

pubs.acs.org/JACS

Highly Symmetric Gold Nanostars: Crystallographic Control and Surface-Enhanced Raman Scattering Property

Wenxin Niu, Yi An Alvin Chua, Weiqing Zhang, Hejin Huang, and Xianmao Lu*

Department of Chemical and Biomolecular Engineering, National University of Singapore, 4 Engineering Drive 4, Singapore 117585

Supporting Information

ABSTRACT: Gold nanostars have attracted widespread interest due to their remarkable properties and broad applications in plasmonics, spectroscopy, biomedicine, and energy conversion. However, current synthetic methods of Au nanostars have limited control over their symmetry; most existing nanostars are characterized by having uncertain number of arms with different lengths and random spatial arrangement. This morphological arbitrariness not only hampers the fundamental understanding of the properties of Au nanostars, but also lead to poor reproducibility in their applications. Here we demonstrate that, by using a robust solution-phase method, Au nanostars with unpreceded degree of symmetry control can be obtained in high yield and with remarkable monodispersity. Icosahedral seeds are used to dictate the growth of 3D evenly distributed arms in an I_h symmetric manner. Alkylamines serve as shape-control agent to regulate the growth of the hexagonal pyramidal arms enclosed by high-index facets. Benefiting from their high symmetry, the Au nanostars exhibit superior single-particle SERS performance compared to asymmetric Au nanostars, in terms of both intensity and reproducibility.

Gold nanocrystals (NCs) have attracted widespread interest for decades due to their remarkable properties that can be finely tailored by their sizes and shapes.[1,2] These unique properties offer the promise of enabling important advances in interdisciplinary areas including plasmonics, spectroscopy, biomedicine, and energy conversion.[3−5] Many of these applications stem from the unique optical properties of Au NCs, which can strongly absorb and scatter light through a well-known phenomenon called localized surface plasmon resonance (LSPR).[6] To optimally harness the plasmonic properties of Au NCs, extensive efforts have been devoted to investigate the controllable synthesis of Au NCs and elucidate their shape-dependent properties.

Among different plasmonic Au NCs, Au nanostars are emerging as a remarkably powerful building block due to their intriguing properties.[7] A gold nanostar could be defined as a branched nanostructure with a central core and several protruding arms with sharp tips.[8−10] The local field strength in the vicinity of the sharp tips of Au nanostars can be enhanced by several orders of magnitude compared with the incident light, providing a basis of plasmon-enhanced spectroscopy.[11] Furthermore, the LSPR of Au nanostars can be easily tuned into the near-infrared (NIR) region of the electromagnetic spectrum,[12] holding great promise for biological applications. Due to these key properties, Au nanostars have been vastly used in sensing, surface enhanced Raman scattering (SERS), biological imaging, nanotherapeutics, and nanomedicine.[13−17] These applications underscore the need for developing Au nanostars with defined shapes and uniform branches. Unfortunately, current methods provide limited control over the structural parameters of Au nanostars. Most nanostars are characterized by their uneven arms of different lengths. Moreover, the numbers of arms are extremely hard to control and the spatial arrangement of the arms around the core is random. These undesired characteristics will lead to unreliable results with poor reproducibility in various applications of Au nanostars and hamper the fundamental understanding of their properties and the assessment of their performance. To fully implement the advantageous properties of Au nanostars, a precise control over their symmetry and uniformity is highly desired.

In this study, a simple solution-phase method was exploited to grow highly symmetric Au nanostars from icosahedral Au seeds in a dimethylformamide (DMF) solution containing polyvinylpyrrolidone (PVP), chloroauric acid, dimethylamine (DMA), and hydrochloric acid (see Supporting Information for details). Transmission electron microscopy (TEM) and scanning electron microscope (SEM) images of the Au nanostars are shown in Figure 1a−c, respectively. The Au nanostars show remarkable monodispersity in terms of both shape and size (Figures 1a and S2). More interestingly, all nanostars are highly symmetric with a projected profile of a decagram featuring ten identical arms (Figure 1d). The angles between two adjacent arms are 36°. Selected area electron diffraction (SAED) pattern of a Au nanostar along its 5-fold axis is the same as that of icosahedral Au NCs and Platonic dodecahedral Au NCs viewed from the same axis,[18−20] demonstrating that Au nanostars have the same icosahedral multiply-twinned structure as their seeds (Figures 1d inset). High-resolution TEM (HRTEM) studies reveal that each arm of the Au nanostar is single-crystalline (Figure S3).

Closer inspection of the SEM images (Figure 1e−j) reveals that there are 20 identical arms on each nanostar and that each arm is a hexagonal pyramid with a sharp tip (animations showing rotating 3D nanostar models are available). More importantly, the 20 arms on a nanostar show a rigid 3D arrangement around its core. Three types of rotational axes were found for the nanostars: 5-fold, 3-fold, and 2-fold axes. Therefore, the

Received: May 22, 2015
Published: August 10, 2015

DOI: 10.1021/jacs.5b05321
J. Am. Chem. Soc. 2015, 137, 10460−10463

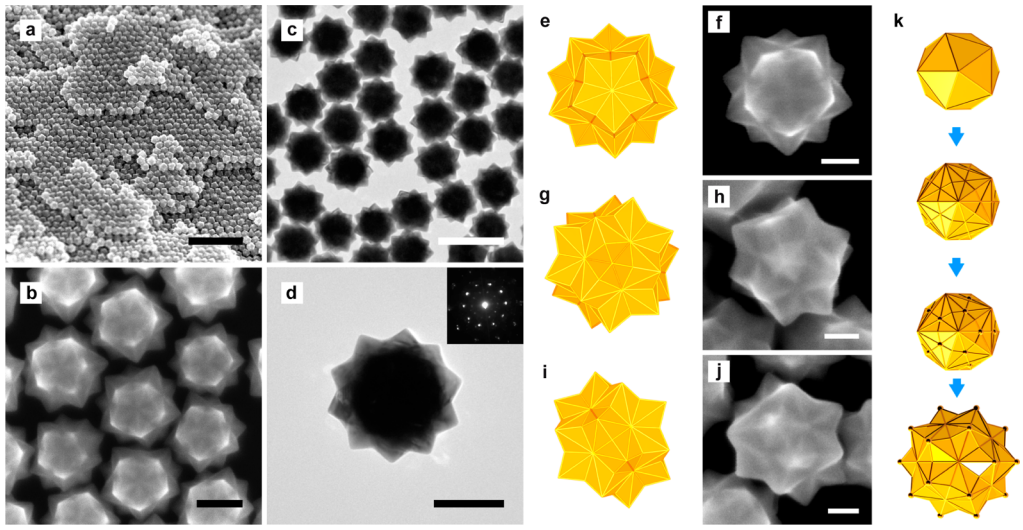

Figure 1. (a–c) SEM and TEM images of monodispersed Au nanostars. (d) TEM image of a single Au nanostar and its corresponding SAED pattern. (e–j) SEM images and corresponding geometric models of Au nanostars viewed from their 5-fold, 3-fold, and 2-fold axes, respectively. (k) Schematic illustration of shape transition from an icosahedron to a nanostar. An animation showing the shape evolution is available. Scale bars: (a) 1 μm; (b) 100 nm; (c) 200 nm; (d) 100 nm; (f,h,j) 50 nm.

nanostars show the same icosahedral (I_h) symmetry with the icosahedral seeds.[18] The highly symmetric Au nanostar in our work could be viewed as a stellated polyhedron composed of 120 facets, 180 edges, and 62 vertices. It obeys the Euler's polyhedron formula: $V + F - E = 2$ (where V is the number of polyhedron vertices, E is the number of polyhedron edges, and F is the number of faces).[21] These nanostars represent one of the most complicated yet symmetric shapes of nanocrystals with well-defined facets.

The strikingly high I_h symmetry of the Au nanostars originates from the icosahedral seeds.[22−24] Based on the symmetry similarity between an icosahedron and a nanostar, we proposed the following steps to construct models for Au nanostars (Figure 1k). First, each triangular face of an icosahedron is equally split up into six faces sharing the center point of the triangle. Upon pulling outward all the center points of the icosahedron, a stellated polyhedron with 20 hexagonal pyramids will form. Building a hexagonal pyramid on {111} facets is known to generate high-index {*hkl*} facets.[25,26] Based on this geometric model, Au nanostars enclosed by different {*hkl*} facets were theoretically predicted (Figure S4). An empirical relationship between the tip sharpness and the {*hkl*} facets is obtained from these models. Typically, smaller h/k and l/k values will lead to Au nanostars with sharper tips. Among different models in Figure S4, the Au nanostars in Figure 1 are in excellent agreement with the model built from {321} facets (Figure S5−S6).

While the high symmetry of the Au nanostars is dictated by its icosahedral seeds, the formation of {321} high-index facets is attributed to the selective adsorption of DMA on Au {321} facets. In order to elucidate the role of DMA, different amounts of DMA are investigated during the NC growth. Figure 2a shows that without DMA, Au dodecahedral NCs enclosed by {110} facets were obtained.[18] As the concentration of DMA increases, the corners of Au dodecahedra became sharper and finally evolved into {321}-faceted arms of the Au nanostars (Figures 2b–f and S7). Relative slow growth kinetics favors the selective adsorption of DMA on Au {321} facets. Either higher reaction temperature or lower concentration of HCl will increase the addition rates of Au atoms on the seeds and inhibit the selective adsorption of DMA on {321} facets. Consequently, Au nanostars

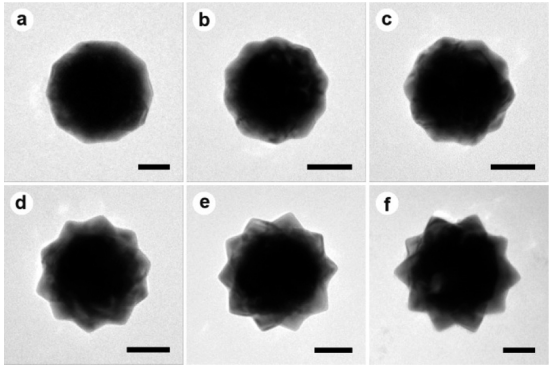

Figure 2. Au NCs synthesized in the presence of different amounts of DMA: (a) 0 μL, (b) 6.3 μL, (c) 12.5 μL, (d) 25 μL, (e) 50 μL, (f) 100 μL of 40% DMA solution. The volume ratio between 40% DMA and 2.5 M HCl solutions was kept at 5:8. Scale bars: 50 nm.

with round corners and ambiguous facets were obtained if the amount of HCl was halved (Figure S8−9) or the reaction temperature was increased by 20 °C (Figure S10).

Noble metal NCs enclosed by high-index facets has received considerate attention in recent years and have been proved to exhibit superior performances in catalysis.[27−32] However, high-index facets usually possess high surface energy and their synthesis is very challenging, especially for the {*hkl*} family.[31,32] Besides DMA, we further discovered that methylamine, ethylamine, butylamine, and octylamine can be also exploited in the synthesis of highly symmetric Au nanostars enclosed with high-index facets (Figures 3 and S11−14). For ethylamine and butylamine, similar nanostars enclosed by {321} facets were obtained. Interestingly, nanostars with less sharper arms were obtained for methylamine, in accordance to the model enclosed by {753} facets. For octylamine, nanostars with sharper arms were obtained, matching the model enclosed by {742} facets. These results demonstrate that alkylamines can be an efficient facet-regulating agent for high-energy {*hkl*} facets of gold NCs. Moreover, the sharpness of Au nanostars can be fine-tuned. The facet-regulating effect of alkylamines was also validated with different Au seeds; when single-crystalline Au octahedra were

DOI: 10.1021/jacs.5b05321
J. Am. Chem. Soc. 2015, 137, 10460−10463

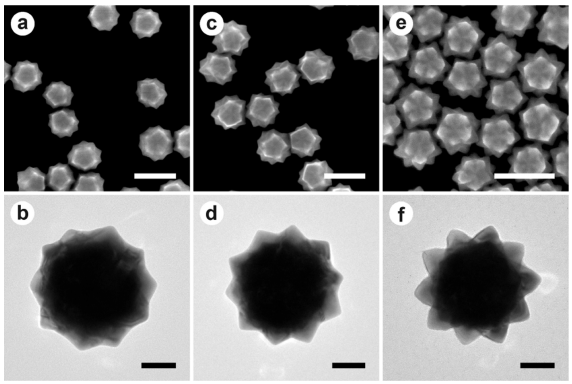

Figure 3. SEM and TEM images of Au nanostars synthesized with different amines: (a,b) methylamine, (c,d) ethylamine, (e,f) octylamine. Scale bars: (a,c,e) 200 nm; (b,d,f) 50 nm.

employed to grow Au NCs in the presence of DMA, hexoctahedral Au NCs enclosed by {321} facets were obtained (Figure S15). In addition to facet and tip sharpness, the size of Au nanostars can also be controlled via additional growth step in which Au nanostars were used as seeds and grown under similar growth conditions (Figure S16).

In the past two decades, renewed interest in SERS has been stimulated by the possibility of controllably synthesizing and assembling of plasmonic NCs.[33−35] Theoretical calculations predicted that the narrow gaps formed when Au sharp tips are brought into proximity with an Au thin film could produce an extremely high local field enhancement, with the possibility of producing a SERS enhancement of 2 orders of magnitude higher than gaps from nanoparticle dimers.[36] Based on this platform, asymmetric Au nanostars has been deposited onto a smooth Au thin film and achieved zeptomolar detection capability.[37] A prerequisite for achieving optimum performance in such a platform, however, is to be able to direct the tips of nanostars pointing down to the gold film. For typical asymmetric nanostars (Figure S17), the optimum construction of such platform is difficult due to their uneven arms with different lengths and random spatial arrangement.[38,39] In contrast, the highly symmetric nanostars offer distinct advantages over asymmetric nanostars. They show exclusive tendency to land on a flat surface with five of its arms, creating five hot spots between the tips and the substrate for SERS measurements (Figure 4a). Our preliminary discrete dipole approximation (DDA) calculations show that symmetric nanostars have higher maximum and average local electromagnetic fields than asymmetric ones (Figure S18). Moreover, asymmetric nanostars exhibit different field enhancements at different orientations, which lead to varied SERS enhance factors (EFs). In this respect, highly symmetric nanostars are expected to have better and more reproducible SERS performance.

To test this hypothesis, a similar star-film platform for SERS was constructed. Ultra large Au nanosheets with atomic flatness were used as gold films.[40] After the Au nanosheets were incubated with 4-mercaptobenzoic acid (MBA) solution, Au nanostars were deposited on the Au nanosheets, and thus forming hot spots with trapped MBA molecules between the Au nanostars and nanosheets (inset of Figure 4a). As the Au nanostars show a strong surface plasmon band at near-infrared (NIR) region (Figure 4b), a 785 nm laser was used to acquire SERS signal. Figure 4c−h shows that the SEM images and optical images of Au nanostars match really well, allowing the focus of

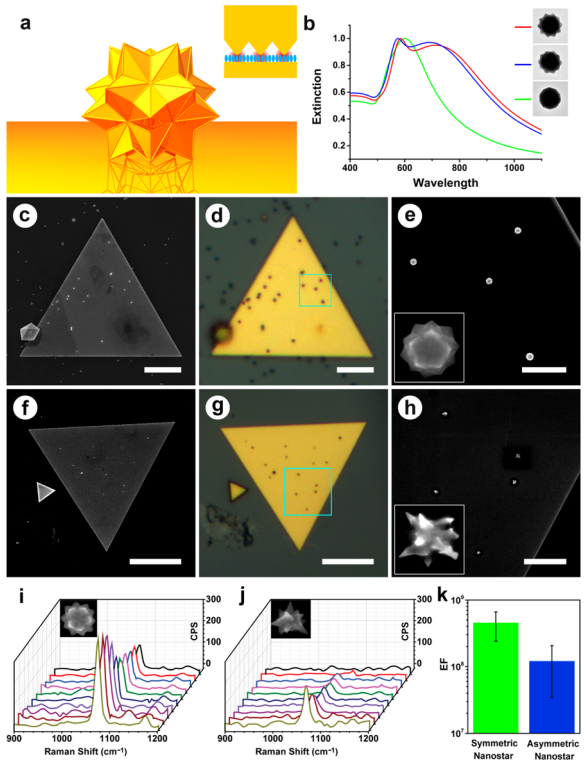

Figure 4. (a) Geometric model of a free-standing Au nanostar on a Au nanosheet. An animation showing a rotating nanostar on substrate is available. The inset shows a schematic of hot spots with trapped MBA molecules between tips of a Au nanostar and a nanosheet. (b) UV−vis−NIR spectra of dodecahedral Au nanocrystals (green curve), Au nanostars with round tips (blue curve), and Au nanostars with sharp tips (red curve). (c−h) SEM and bright field optical images of Au nanostars on Au nanosheets: (c−e) symmetric Au nanostars, (f−h) asymmetric Au nanostars. The insets of (e) and (h) are two single nanostars. (i,j) SERS spectra of MBA from symmetric and asymmetric Au nanostars, respectively. (k) Average EFs of symmetric and asymmetric Au nanostars. Scale bars: (c,d) 5 μm, (f,g) 10 μm, (e) 1 μm, (h), 2 μm.

the 785 nm laser on a single nanostar during SERS measurements. Single-particle SERS spectra of ten representative well-isolated symmetric and asymmetric Au nanostars were measured, as shown in Figure 4i,j, respectively. The symmetric Au nanostars exhibit much better SERS performance than the asymmetric Au nanostar. The symmetric Au nanostars show both higher single-particle SERS intensity and better reproducibility than asymmetric Au nanostars (Figure 4k). The enhance factors for symmetric Au nanostars range from 2.3−7.5 $\times$ 10^8 with an average of 4.5 $\times$ 10^8, nearly four times stronger than that of asymmetric nanostars (1.7 $\times$ 10^7−2.9 $\times$ 10^8, average 1.2 $\times$ 10^8). For symmetric nanostars, all the EF factors of the symmetric nanostars are in the same order; the largest EF is only three times as large as the smallest one. While the EF factors of asymmetric nanostars vary in 2 orders of magnitude, the largest EF is over 17 times greater than the smallest one. Statistically, the symmetric nanostars have much lower relative standard deviation than the asymmetric nanostars (46.7% vs 71.2%), indicating that the symmetric nanostars have higher reproducibility in their SERS performance. Moreover, the EF values could be underestimated because all the molecules beneath the nanostar were considered for SERS herein, while actually only the molecules trapped in the proximity to the tips of Au nanostars contribute to the SERS performances.[41]

DOI: 10.1021/jacs.5b05321
J. Am. Chem. Soc. 2015, 137, 10460−10463

In conclusion, Au nanostars with unpreceded high degree of symmetry were synthesized in high yield and remarkable monodispersity. Icosahedral seeds were used to dictate the I_h symmetry of the nanostars. DMA, along with other alkylamines, was found to stabilize the high-index {*hkl*} Au facets for the first time. Benefiting from their high symmetry, the Au nanostars exhibit superior single-particle SERS performance in terms of both intensity and reproducibility. The remarkable level of synthetic control of highly symmetric nanostars demonstrates that increased sophistication in shape-selective growth of plasmonic nanomaterials could be achieved by tailored nucleation and growth and implied future development of programmed synthesis of nanoarchitectures. As a result of their high symmetry and uniformity, these nanostars will provide exciting new opportunities to study the fundamental plasmonic properties of shaped NCs and enrich the choices of building blocks for NC assemblies. Their near-IR LSPR properties also endow the Au nanostars great potential in biological applications.

■ ASSOCIATED CONTENT

Supporting Information

The Supporting Information is available free of charge on the ACS Publications website at DOI: 10.1021/jacs.5b05321.

Detailed experimental procedures, additional TEM and SEM images, models of Au nanostars enclosed by different {*hkl*} high-index facets, and UV−vis spectra of Au nanostars (PDF)

Nanostar rotating along 2-fold axis (AVI)

A randomly rotating nanostar (AVI)

Shape evolution from icosahedron to nanostar (AVI)

Nanostar rotating on flat substrate (AVI)

■ AUTHOR INFORMATION

Corresponding Author

*chelxm@nus.edu.sg

Notes

The authors declare no competing financial interest.

■ ACKNOWLEDGMENTS

We thank Ministry of Education Singapore (Grant #R279-000-391-112), Singapore National Research Foundation (Grant# R279-000-337-281), and French-Singaporean joint MERLION program (Grant# R279-000-334-646) for the financial support of this work.

■ REFERENCES

(1) Eustis, S.; El-Sayed, M. A. *Chem. Soc. Rev.* **2006**, *35*, 209.

(2) Grzelczak, M.; Perez-Juste, J.; Mulvaney, P.; Liz-Marzan, L. M. *Chem. Soc. Rev.* **2008**, *37*, 1783.

(3) Lu, X.; Rycenga, M.; Skrabalak, S. E.; Wiley, B.; Xia, Y. *Annu. Rev. Phys. Chem.* **2009**, *60*, 167.

(4) Linic, S.; Christopher, P.; Ingram, D. B. *Nat. Mater.* **2011**, *10*, 911.

(5) Saha, K.; Agasti, S. S.; Kim, C.; Li, X.; Rotello, V. M. *Chem. Rev.* **2012**, *112*, 2739.

(6) Chen, H.; Shao, L.; Li, Q.; Wang, J. *Chem. Soc. Rev.* **2013**, *42*, 2679.

(7) Guerrero-Martínez, A.; Barbosa, S.; Pastoriza-Santos, I.; Liz-Marzán, L. M. *Curr. Opin. Colloid Interface Sci.* **2011**, *16*, 118.

(8) Burt, J. L.; Elechiguerra, J. L.; Reyes-Gasga, J.; Montejano-Carrizales, J. M.; Jose-Yacaman, M. *J. Cryst. Growth* **2005**, *285*, 681.

(9) Cabrera-Trujillo, J.; Montejano-Carrizales, J.; Rodríguez-López, J.; Zhang, W.; Velázquez-Salazar, J.; José-Yacamán, M. *J. Phys. Chem. C* **2010**, *114*, 21051.

(10) Jiang, L.; Tang, Y.; Liow, C.; Wu, J.; Sun, Y.; Jiang, Y.; Dong, Z.; Li, S.; Dravid, V. P.; Chen, X. *Small* **2013**, *9*, 705.

(11) Nehl, C. L.; Liao, H.; Hafner, J. H. *Nano Lett.* **2006**, *6*, 683.

(12) Yuan, H.; Khoury, C. G.; Hwang, H.; Wilson, C. M.; Grant, G. A.; Vo-Dinh, T. *Nanotechnology* **2012**, *23*, 075102.

(13) Rodríguez-Lorenzo, L.; de La Rica, R.; Álvarez-Puebla, R. A.; Liz-Marzán, L. M.; Stevens, M. M. *Nat. Mater.* **2012**, *11*, 604.

(14) Li, M.; Kang, J. W.; Dasari, R. R.; Barman, I. *Angew. Chem.* **2014**, *126*, 14339.

(15) Yuan, H.; Fales, A. M.; Vo-Dinh, T. *J. Am. Chem. Soc.* **2012**, *134*, 11358.

(16) Dam, D. H. M.; Lee, R. C.; Odom, T. W. *Nano Lett.* **2014**, *14*, 2843.

(17) Dam, D. H. M.; Lee, J. H.; Sisco, P. N.; Co, D. T.; Zhang, M.; Wasielewski, M. R.; Odom, T. W. *ACS Nano* **2012**, *6*, 3318.

(18) Niu, W.; Zhang, W.; Firdoz, S.; Lu, X. *J. Am. Chem. Soc.* **2014**, *136*, 3010.

(19) Kuo, C.-H.; Hua, T.-E.; Huang, M. H. *J. Am. Chem. Soc.* **2009**, *131*, 17871.

(20) Wang, W.-C.; Lyu, L.-M.; Huang, M. H. *Chem. Mater.* **2011**, *23*, 2677.

(21) Richeson, D. S. *Euler's Gem: The Polyhedron Formula and the Birth of Topology*; Princeton University Press: Princeton, NJ, 2012.

(22) Kim, D. Y.; Yu, T.; Cho, E. C.; Ma, Y.; Park, O. O.; Xia, Y. *Angew. Chem., Int. Ed.* **2011**, *50*, 6328.

(23) Weiner, R. G.; Skrabalak, S. E. *Angew. Chem., Int. Ed.* **2015**, *54*, 1181.

(24) DeSantis, C. J.; Skrabalak, S. E. *J. Am. Chem. Soc.* **2012**, *135*, 10.

(25) Hong, J. W.; Lee, S.-U.; Lee, Y. W.; Han, S. W. *J. Am. Chem. Soc.* **2012**, *134*, 4565.

(26) Zhang, L.; Zhang, J.; Kuang, Q.; Xie, S.; Jiang, Z.; Xie, Z.; Zheng, L. *J. Am. Chem. Soc.* **2011**, *133*, 17114.

(27) Zhou, Z.-Y.; Tian, N.; Li, J.-T.; Broadwell, I.; Sun, S.-G. *Chem. Soc. Rev.* **2011**, *40*, 4167.

(28) Zhang, L.; Niu, W.; Xu, G. *Nano Today* **2012**, *7*, 586.

(29) Quan, Z.; Wang, Y.; Fang, J. *Acc. Chem. Res.* **2012**, *46*, 191.

(30) Jiang, Q.; Jiang, Z.; Zhang, L.; Lin, H.; Yang, N.; Li, H.; Liu, D.; Xie, Z.; Tian, Z. *Nano Res.* **2011**, *4*, 612.

(31) Zhang, L.; Niu, W.; Gao, W.; Qi, L.; Lai, J.; Zhao, J.; Xu, G. *ACS Nano* **2014**, *8*, 5953.

(32) Xiao, J.; Liu, S.; Tian, N.; Zhou, Z.-Y.; Liu, H.-X.; Xu, B.-B.; Sun, S.-G. *J. Am. Chem. Soc.* **2013**, *135*, 18754.

(33) Banholzer, M. J.; Millstone, J. E.; Qin, L.; Mirkin, C. A. *Chem. Soc. Rev.* **2008**, *37*, 885.

(34) Li, J. F.; Huang, Y. F.; Ding, Y.; Yang, Z. L.; Li, S. B.; Zhou, X. S.; Fan, F. R.; Zhang, W.; Zhou, Z. Y.; Ren, B. *Nature* **2010**, *464*, 392.

(35) Lim, D.-K.; Jeon, K.-S.; Hwang, J.-H.; Kim, H.; Kwon, S.; Suh, Y. D.; Nam, J.-M. *Nat. Nanotechnol.* **2011**, *6*, 452.

(36) Alvarez-Puebla, R.; Liz-Marzán, L. M.; García de Abajo, F. J. *J. Phys. Chem. Lett.* **2010**, *1*, 2428.

(37) Rodríguez-Lorenzo, L.; Álvarez-Puebla, R. A.; Pastoriza-Santos, I.; Mazzucco, S.; Stéphan, O.; Kociak, M.; Liz-Marzán, L. M.; García de Abajo, F. J. *J. Am. Chem. Soc.* **2009**, *131*, 4616.

(38) Fales, A. M.; Yuan, H.; Vo-Dinh, T. *J. Phys. Chem. C* **2014**, *118*, 3708.

(39) Sau, T. K.; Murphy, C. J. *J. Am. Chem. Soc.* **2004**, *126*, 8648.

(40) Li, C. C.; Cai, W. P.; Cao, B. Q.; Sun, F. Q.; Li, Y.; Kan, C. X.; Zhang, L. D. *Adv. Funct. Mater.* **2006**, *16*, 83.

(41) Fang, Y.; Seong, N.-H.; Dlott, D. D. *Science* **2008**, *321*, 388.

DOI: 10.1021/jacs.5b05321
J. Am. Chem. Soc. 2015, 137, 10460−10463